J Electr Eng Technol Vol. 9, No. 3: 827-834, 2014
http://dx.doi.org/10.5370/JEET.2014.9.3.827

ISSN(Print) 1975-0102
ISSN(Online) 2093-7423

Fault Response of a DFIG-based Offshore Wind Power Plant Taking into Account the Wake Effect

Jinho Kim*, Jinsik Lee*, Yongsug Suh, Byongjun Lee*** and Yong Cheol Kang†**

Abstract – In order to meet the low voltage ride-through requirement in a grid code, a wind power plant (WPP) has to stay connected to a grid, supporting the voltage recovery for a grid fault. To do this, a plant-level controller as well as a wind generator (WG) controller is essential. The dynamic response of a WPP should be analyzed in order to design a plant-level controller. The dynamic response of a WPP for a grid fault is the collective response of all WGs, which depends on the wind speed approaching the WG. Thus, the dynamic response of a WPP should be analyzed by taking the wake effect into consideration, because different wind speeds at WGs will result in different responses of the WPP. This paper analyzes the response of a doubly fed induction generator (DFIG)-based offshore WPP with a grid fault taking into account the wake effect. To obtain the approaching wind speed of a WG in a WPP, we considered the cumulative impact of multiple shadowing and the effect of the wind direction. The voltage, reactive power, and active power at the point of common coupling of a 100 MW DFIG-based offshore WPP were analyzed during and after a grid fault under various wind and fault conditions using an EMTP-RV simulator. The results clearly demonstrate that not considering the wake effect leads to significantly different results, particularly for the reactive power and active power, which could potentially lead to incorrect conclusions and / or control schemes for a WPP.

Keywords: DFIG, Voltage control, Wake effect, LVRT requirement, Crowbar and Grid fault.

1. Introduction

Due to the technical advances and financial viability of wind generation, wind power installations have been increasing in size globally [1]. The installed capacity of wind generators (WGs) worldwide is expected to increase to 832 GW by 2020 [2]. Variable-speed wind generators (VSWGs) have been widely used to maximize energy extraction from the wind [3, 4]. A doubly-fed induction generator (DFIG) shares approximately 50% of the wind energy market [5].

The voltage and frequency in a grid should be maintained within the acceptable ranges at all times for the stable operation. The grid frequency is a global variable and is maintained by adjusting the output of any of the generators in the grid. On the other hand, the voltage at a node is a local variable and, therefore, is controlled by a local generator or the compensating unit closest to the applicable node. For a power system with high wind penetration, wind generators should be able to support the voltage when a disturbance occurs in the system.

In the past, a WG was allowed to be tripped out to protect itself when a fault occurs in a grid. However, as the wind penetration increases, WGs should stay connected to the grid for a grid fault. This function is known as the low voltage ride-through (LVRT) requirement. To comply with this requirement, a wind power plant (WPP) should not only be able to withstand the fault, but also to support the reactive power during the fault and after the fault clearance [6]. To do this, a plant-level controller and a wind generator (WG) controller are essential. The dynamic response of a WPP during the fault and after the fault clearance should be analyzed when designing a plant-level controller.

The dynamic response of a WPP for a grid fault is the collective response of all of the WGs, which depends on the wind speed approaching the WGs. Thus, the dynamic response of a WPP should be analyzed by taking the wake effect into consideration, particularly for a grid fault. This is because different wind speeds approaching WGs will result in different operating conditions of the WGs such as the active power and reactive power support capabilities, which result in different dynamic responses of the WPPs.

Many researches on the dynamic responses of WPPs for grid faults have been reported [7-11]. A detailed analytical analysis of a DFIG was implemented for a comprehensive

† Corresponding Author: Dept. of Electrical Engineering, WeGAT Research Center, and Smart Grid Research Center, Chonbuk National University, Korea. (yckang@jbnu.ac.kr)
* Dept. of Electrical Engineering and WeGAT Research Center, Chonbuk National University, Korea. ({jkim, 2jinshik}@jbnu.ac.kr)
** Dept. of Electrical Engineering, WeGAT Research Center, and Smart Grid Research Center, Chonbuk National University, Korea. (ysuh@jbnu.ac.kr)
*** Dept. of Electrical Engineering, Korea University, Korea. (leeb@korea.ac.kr)
Received: February 9, 2014; Accepted: February 24, 2014

understanding of its fault response [7, 8]. The effect of a grid fault on a DFIG was demonstrated, and control strategies for its stable recovery were suggested [9, 10]. The response of a DFIG-based WPP was analyzed in terms of the reactive power support capabilities, in compliance with a grid code [11]. These studies assumed that a WPP behaves like a single WG. However, the modeling of a WPP as multiple units of WGs and the consideration of the wake effect are essential in order to obtain a realistic dynamic response of a WPP for a grid fault.

This paper analyzes the dynamic response of a DFIG-based offshore WPP for a grid fault, considering the wake effect. To obtain the approaching wind speed of a WG in a WPP, we considered the cumulative impact of multiple shadowing and the effect of the wind direction. The voltage, reactive power, and active power at the point of common coupling (PCC) of a 100 MW DFIG-based offshore WPP were analyzed during and after a grid fault under various wind and fault conditions using an EMTP-RV simulator.

2. Fault Response of a DFIG-based Offshore Wind Power Plant Taking into Account the Wake Effect

2.1 Control strategies of a DFIG for a grid fault

As specified in the Korean grid code, a WPP of more than 20 MW should meet the LVRT requirement (Fig. 1). To comply with this requirement, WPPs should remain connected to the grid for a specified time period depending on the voltage dip.

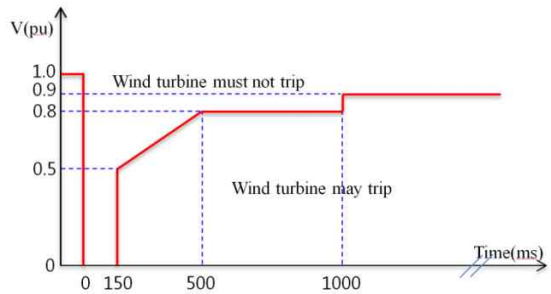

Fig. 1. Korean LVRT requirement

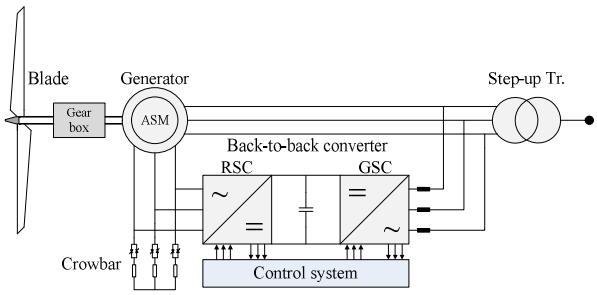

Fig. 2. Configuration of a DFIG

If the terminal voltage of a DFIG drops due to a grid fault, the flux in the stator winding of the DFIG decreases. Immediately after the fault occurrence, the magnetic energy that has been stored in the magnetic field is released in the form of an overcurrent in the rotor circuit, which causes an overvoltage across a dc-link by charging the dc-link capacitor, resulting in damage to the converters, unless some form of protection is provided. A crowbar is commonly used to protect the converters in DFIGs [12].

Fig. 2 shows a typical configuration of a DFIG that was used in this paper. Figs. 3 and 4 show the control schemes for the rotor side converter (RSC) and the grid side converter (GSC), respectively. The RSC controls the active and reactive powers in a stator winding using two loops. The top loop shown in Fig. 3 was used to maximize the stator active power through a maximum power point tracking (MPPT) control. In this paper, the reference for the MPPT control P_{G_ref} was set to (1) as in [13]

$$P_{G\_ref} = k_g \omega_r^3 \tag{1}$$

where k_g is a function of the parameters, such as the gear-ratio, blade length, blade profile, etc.

The bottom loop shown in Fig. 3 was employed either to keep the stator terminal voltage as a nominal value or to inject the reactive power into the grid.

On the other hand, the top loop shown in Fig. 4 was used to control the dc-link voltage, while the bottom loop shown in Fig. 4 was used to inject the reactive power into the grid. Alternatively, the GSC only maintains the dc-link voltage as a constant without a reactive power injection. To do this, the power flowing into the dc-link P_{dc} of (2) should be equal to the output power of the dc-link.

$$P_{dc} = \frac{dW_c}{dt} = \frac{1}{2} C_{dc} \frac{dV_{dc}^2}{dt} \tag{2}$$

where W_c is the energy stored in the dc capacitor, C_{dc}.

In the case of a severe grid fault, if the RSC is blocked,

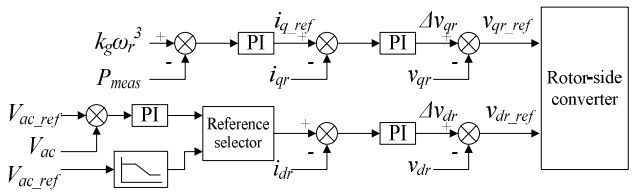

Fig. 3. RSC control scheme

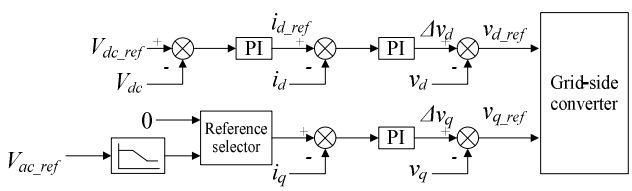

Fig. 4. GSC control scheme

only the GSC can inject the reactive power into the grid [14]. In this paper, both the RSC and GSC inject the reactive power into the grid for voltage support if the terminal voltage of the DFIG dropped by more than 10 % of its nominal value, and the reactive current of 1 pu was injected for a voltage below 50 % of the rated voltage [15].

In this paper an active crowbar was also included in the DFIG, because the activation of crowbars affects its response. This device shorts the rotor windings through its resistors. Careful attention should be paid when choosing the resistance, which affects the behavior of the rotor current. The large resistance in the crowbar leads to the effective damping of the rotor and stator overcurrent; however, if the resistance is too large, an overvoltage across the resistance may occur. As in [16], this paper calculated the crowbar resistance using:

$$R_{CB} = \frac{\sqrt{2}V_{r\_\max}\omega_e L_s'}{\sqrt{3.2V_s^2 - 2(v_{r\_\max})^2}}$$
$$L_s' = L_s + \frac{L_r L_m}{L_r + L_m} \tag{3}$$

where V_{r_max} is the maximum rotor voltage, ω_e is the synchronous angular frequency, L_s is the stator inductance, L_r is the rotor inductance, L_m is the magnetizing inductance, and V_s is the stator voltage.

Fig. 5 shows the crowbar activation logic used in this paper. If either the instantaneous rotor current or the dc-link voltage exceeded the threshold value, the rotor circuit was shorted through the crowbar resistors and, simultaneously, the RSC was disconnected from the DFIG. In this case, the RSC would have been unable to control the stator active and reactive powers and, thus, the DFIG would become an induction machine. Once the rotor current or dc-link voltage was reduced below the threshold value, the crowbar circuit was disconnected from the rotor winding. At the same time, the RSC was reconnected to the rotor winding and the RSC regained its controllability.

2.2 Calculation of the wake wind speed [17]

In order to analyze the dynamic response of a WPP for a grid fault, the wind speeds approaching all WGs should be obtained. To achieve this, we calculated the wake wind speed at WGs using the method suggested in [17], because it considers the cumulative impact of multiple shadowing and the effect of the wind direction.

WGs in a WPP generate electricity by extracting the kinetic energy in the wind. The upstream WGs will impact the wind speed at other WGs further downstream. This shadowing effect is known as the wake effect [17].

For a simple case of a WG and its shadow cone, Fig. 6, where we assume a steady-state air flow, the wake wind speed at x, $v_w(x)$ can be obtained on the basis of the mass conservation principle, i.e.,:

$$\pi r_{rot}^2 v_{w0} + \pi(r(x)^2 - r_{rot}^2)v_0 = \pi r(x)^2 v_w(x) \tag{4}$$

In (4), $r(x)$ can be calculated using:

$$r(x) = r_{rot} + x\tan\alpha \tag{5}$$

The factor tan α in (5) may have two possible values depending on the nature of the incoming wind. For a free wind, tan α is set to 0.04; otherwise, it should be set to 0.08 [18].

Solving (4) gives $v_w(x)$, i.e.,

$$v_w(x) = \frac{r_{rot}^2}{r^2}v_{w0} + \{1 - \frac{r_{rot}^2}{r(x)^2}\}v_0$$
$$= v_0 + (v_{w0} - v_0)\{\frac{r_{rot}}{r(x)}\}^2 \tag{6}$$

Now, as a general case, we assume that a WPP consists of multiple units of WGs, as shown in Fig. 7. In this case, a WG might experience multiple wakes with different degrees of shadowing, depending on the location and wind direction. Therefore, the overlapping area between the corresponding WGs should be taken into account when calculating the wind speed of a WG. Thus, the resultant wind speed of a WG$_j$, v_j, can be obtained by:

$$v_j = v_{j0} - \sqrt{\sum_{\substack{k=1 \\ k\neq j}}^{n} \beta_k \{v_{wk}(x_{kj}) - v_{j0}\}^2} \tag{7}$$

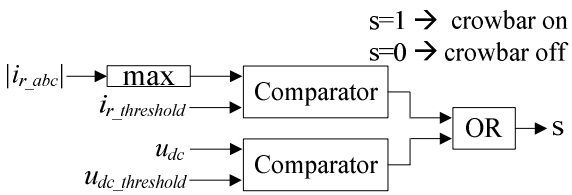

Fig. 5. Logic for activating an active crowbar

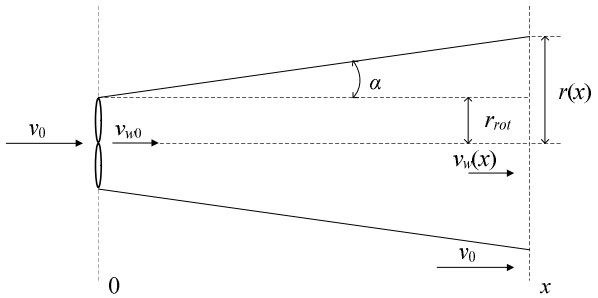

x : radial distance between the WG and an arbitrary location
r_{rot} : radius of the upstream WG
$r(x)$: radius of the shadow cone
α : apex factor of the cone
v_0, v_{w0} : free wind speed and leeside wind speed
$v_w(x)$: wake wind speed at x inside the cone

Fig. 6. Shadow cone of a WG

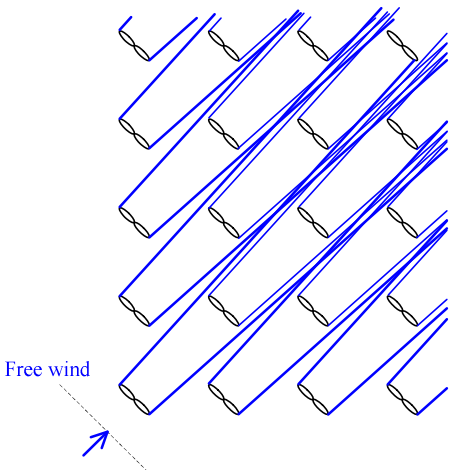

Fig. 7. Multiple wakes in a WPP

where v_{j0} is the incoming wind speed at WG_j without any shadowing, x_{kj} is the radial distance between WG_k and WG_j, $v_{wk}(x_{kj})$ is the speed of the wind approaching WG_j from the shadowing WG_k, β_k is the ratio of an area of WG_j under the shadow of WG_k to its total area, and n is the total number of WGs.

2.3 Impacts of the wake effect on operating conditions of DFIGs and reactive powers of the submarine cables

In a WPP, the wind speed arriving at downstream WGs might be slightly different from that of the upstream WG. However, the aerodynamic powers P_{air} can differ significantly, because it is proportional to the cube of the wind speed, i.e.,

$$P_{air} = \frac{1}{2}\rho A v^3 \tag{8}$$

where ρ is the air density in kg/m^3, A is the interception area in m^2, and v is the wind speed in m/s.

In order to extract the maximum power from the wind, the DFIGs operate in a MPPT mode through the speed control mode, where the tip speed ratio of a DFIG is kept as:

$$\lambda_{\text{opt}} = \frac{\omega_{r\_opt} R}{v} \tag{9}$$

where ω_{r_opt} is the optimal rotor speed in rad/s, and R is the blade length in m. Due to the differing wind speeds arriving at DFIGs, the DFIGs operate at different rotor speeds.

The slip is defined as:

$$s = \frac{\omega_s - \omega_r}{\omega_s} \tag{10}$$

where ω_s and ω_r are the synchronous speed in rad/s and the rotor speed in rad/s, respectively.

The rotor voltage V_r and active power of the rotor P_r also depends on the slip as follows:

$$|V_r| = s|V_s| \tag{11}$$

$$P_r = -sP_s \tag{12}$$

where V_s and P_s are the stator voltage and the stator active power, respectively.

Consequently, the total active power from the DFIG to the grid P_G depends on the slip as follows:

$$P_G = P_s - sP_s = (1-s)P_s \tag{13}$$

On the other hand, the reactive power of the DFIG depends on the slip and the DFIG's rotor reactive power, referred to the stator, can be expressed as:

$$Q_r^{'} = \text{Im}\left[\frac{V_r I_r^*}{s}\right] \tag{14}$$

where I_r is the rotor current.

Moreover, in the case of an offshore WPP, the submarine cables either supply or consume the reactive power, depending on the voltage and current, which varies due to the wake effects. Thus, the reactive powers of the cables influence the reactive power at the PCC of a WPP.

Consequently, the wake effect will impact the reactive power of the cable, as well as the active power and reactive power of DFIGs. This, in turn, impacts the response of a WPP consisting of multiple units of DFIGs.

3. Case Studies

3.1 Model system

Fig. 8 shows a model system that includes an offshore WPP connected to the grid. The offshore WPP consists of 20 units of a 5 MW DFIG. The four DFIGs are connected to each feeder through 2.3kV/33kV transformers. The five collector feeders are connected to the 33/154 kV

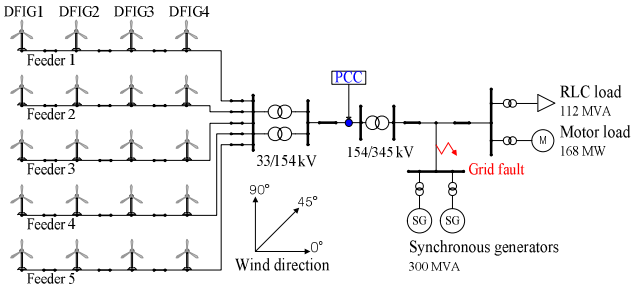

Fig. 8. Model system configuration

Table 1. Wind speeds at all WGs in the WPP

Wind speed w/o wake (m/s)			
12.00	12.00	12.00	12.00
12.00	12.00	12.00	12.00
12.00	12.00	12.00	12.00
12.00	12.00	12.00	12.00
12.00	12.00	12.00	12.00

Wind speed for 0 deg(m/s)			
12.00	11.41	10.69	9.71
12.00	11.41	10.69	9.71
12.00	11.41	10.69	9.71
12.00	11.41	10.69	9.71
12.00	11.41	10.69	9.71

Wind speed for 45 deg (m/s)			
12.00	11.62	11.18	10.59
12.00	11.62	11.18	10.59
12.00	11.62	11.18	11.18
12.00	11.62	11.62	11.62
12.00	12.00	12.00	12.00

Wind speed for 90 deg (m/s)			
8.34	8.34	8.34	8.34
9.71	9.71	9.71	9.71
10.69	10.69	10.69	10.69
11.41	11.41	11.41	11.41
12.00	12.00	12.00	12.00

substation transformer through the 33 kV submarine cables and then to the PCC through the 10 km 154 kV submarine cable. The distance between two neighboring DFIGs was set to 1km. The grid consists of two 150 MVA synchronous generators (SGs) and a motor load of 168 MW and a RLC load of 112 MVA. In the system, the motor load shares 60% of the total load. We assumed that the SGs are steam turbine generators with a steam governor droop of 5%. The threshold of the current and dc voltages for activating an active crowbar was set to 1.5 pu and 1.1 pu, respectively.

3.2 Analysis of the dynamic response of a WPP

In order to take the wake effect into account, the wind speeds approaching a WG were calculated using (7) for wind directions of 0 deg, 45 deg and 90 deg. Table 1 shows the estimated wind speeds of all of the WGs, where the free wind speed was set to 12 m/s.

Meanwhile, in order to analyze the dynamic response of a DFIG-based WPP which would meet the LVRT requirements stipulated in Korea's grid code, 0 pu and 0.6 pu voltage dip faults were simulated by varying the fault resistance and fault duration time. For a grid fault, a three phase symmetrical fault was applied to a node in the grid. The voltages, reactive powers, and active powers at the PCC were analyzed during the fault and after the fault clearance.

Case 1: 0 pu voltage dip fault for 150 ms duration

Fig. 9 shows the results for case 1, where a fault with a fault resistance of 0 occurred at 7 s, to simulate a 0 pu voltage dip fault, and lasted for 150 ms. Figs. 9(a)-(c) indicate the voltages, the reactive powers, and the active powers at the PCC, respectively. As shown in Fig. 9(a), the voltage for the no wake effect was similar to those of the wind directions of 0 deg, 45 deg, and 90 deg during the fault period. However, after the fault clearance, the voltage for the no wake was different than the voltages at 0 deg, 45 deg and 90 deg. It appears that the voltage for the no wake effect successfully recovered the voltage before the

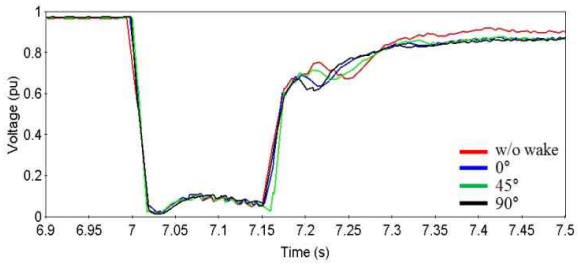

(a) Voltages at the PCC

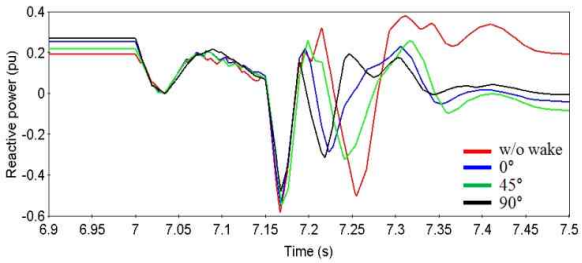

(b) Reactive powers at the PCC

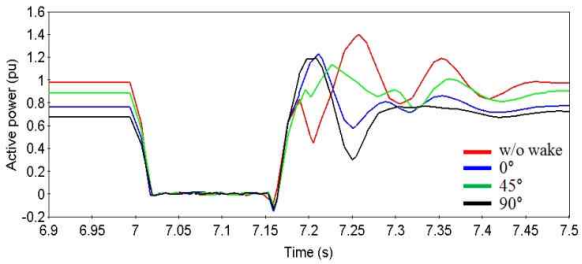

(c) Active powers at the PCC

Fig. 9. Results for case 1

fault occurrence. However, when the wake effects are considered, the results differ, depending on the wind direction, showing slower and less recovery to the nominal voltage. The reason for this slow voltage recovery is that the motor load consumes a large amount of the reactive power after a fault clearance.

The reactive power and active power at the PCC for the no wake effect are similar to those of the other cases during the fault period. However, after the fault clearance, the reactive power and active power for the no wake are distinct from those seen in the other cases, except for the short period immediately following the fault clearance. The difference between the no wake effect and the wake effect implies that the wake effect should be taken into consideration in order to obtain realistic results.

In this case, the fault was so severe that crowbars were activated after the fault clearance, as well as for the period of fault duration (Fig. 10). The RSC was disconnected and the GSC changed the control schemes to inject the reactive power depending on the voltage profile. Therefore, after the fault clearance, the results for the no wake effect differed from those of the other cases, which may lead to incorrect control schemes.

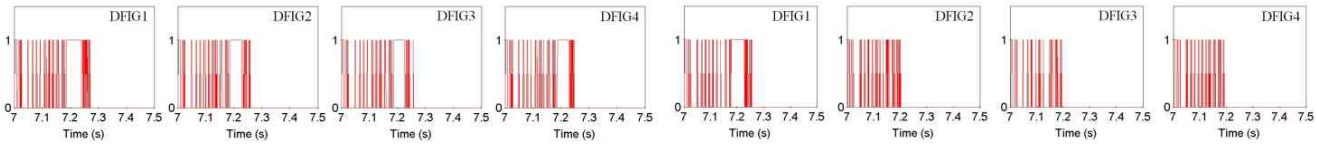

(a) Crowbar signals of the four DFIGs for w/o

(b) Crowbar signals of the four DFIGs for 0°

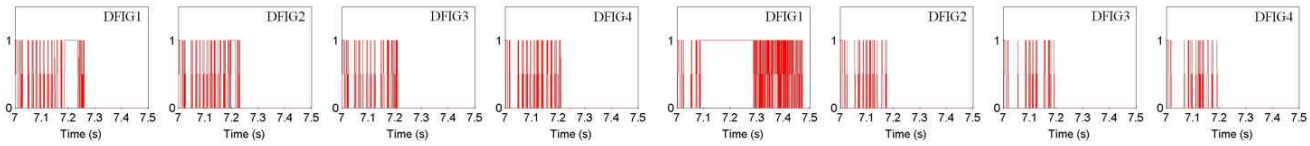

(c) Crowbar signals of the four DFIGs for 45°

(d) Crowbar signals of the four DFIGs for 90°

Fig. 10. Crowbar signals for DFIGs in Feeder 1

Case 2: 0.6 pu voltage dip fault for 250 ms duration

In case 2, a fault with a resistance of 60 Ω occurred at 7 s, to simulate a 0.6 pu voltage dip fault, and lasted for 250 ms (Fig. 11). Figs. 11(a)-(c) show the voltages, the reactive powers, and active powers at the PCC, respectively. In this case, the PCC voltage dropped to 0.6 pu, which was not low enough to trigger the crowbars; therefore, the response of the DFIGs after the fault clearance, as well as during the fault, depended on the control schemes of the RSCs and GSCs. This explains why the crowbar activation signals were not shown herewith.

In this case, the voltages for the no wake effect are similar to those of the wind directions of 0 deg, 45 deg, and 90 deg, while the reactive power and active power for the no wake effect differed from those of the other cases. This is because, in this case, the fault was not severe enough to activate the crowbars; thus, the RSCs were not disconnected from the DFIGs. When the fault was cleared at 7.25 s, the PCC voltage experienced a recovery (Fig. 11a). In addition, neither the instantaneous rotor currents nor the dc-link voltages exceeded the threshold. Moreover, the voltage also recovered slowly, due to the large motor load, as in the previous case.

During the fault period, both RSCs and GSCs changed their control schemes for injecting the reactive power, depending on the voltage profile. In this case, the injected reactive powers supplied by the DFIGs were the same, as they had identical voltage dips; however, the reactive powers at the PCC of the WPP differed with the various wind directions, because the reactive power consumed by the cable impacts the reactive power at the PCC depending on the wake effect. After the fault clearance, the WPP consumed the reactive power for the excitation of the DFIGs for a period of time (see Fig. 11b).

Immediately after the fault occurrence, the active powers at the PCC were significantly reduced; however, with the help of the control of the RSC, they recovered to the values they had prior to the fault occurrence before the fault clearance. This is because the DFIGs were operating in an MPPT mode, even for the reduced terminal voltage, and

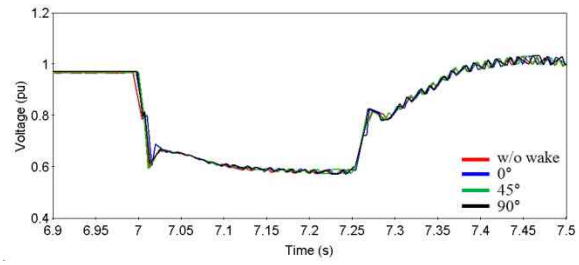

(a) Voltages at the PCC

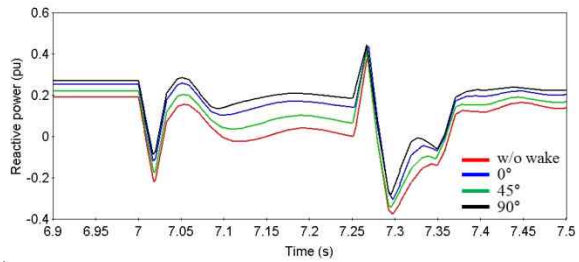

(b) Reactive powers at the PCC

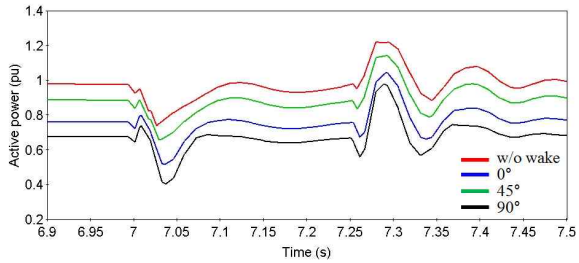

(c) Active powers at the PCC

Fig. 11. Results for case 2

can therefore recover to their original values before the fault occurrence.

Among the three wind directions, the wake effect for the direction of 45 deg was minimal. In this case, the active power of the WPP was the largest, while the reactive power was the smallest, since the cables consume more reactive power than for the other two cases. Therefore, different control algorithms, in terms of active power and reactive power, should be designed depending on the wind

direction.

The aforementioned results clearly demonstrate that the wake effects should be considered when analyzing the dynamic response of a WPP; otherwise researchers might come to incorrect conclusions and suggest flawed solutions for controlling the WPP.

5. Conclusion

This paper analyzed the dynamic response of a DFIG-based offshore WPP with a grid fault, taking into account the wake effects. To obtain the approaching wind speed of a WG in a WPP, the cumulative impact of multiple shadowing and the effect of wind direction were considered. In addition, to analyze the dynamic behavior of a DFIG based offshore WPP for a grid fault, we implemented the functions to meet the LVRT requirements with the reactive power support capability in the grid code in both the RSC and the GSC controllers of the DFIG. Moreover, an active crowbar was included in the DFIG model.

The voltages, reactive powers, and active powers at the PCC of a DFIG-based offshore WPP were analyzed under various fault conditions and wind directions. For the two faults, the voltages for the no wake condition showed patterns similar to those seen for conditions in which the wake effects during the fault and after the fault clearance were considered. However, for the 0 pu voltage fault, the reactive power and active powers showed similar patterns during the fault period, while for the 0.6 pu voltage fault, they showed different patterns, depending on the wake effects. For the 0.6 pu voltage fault, on the other hand, the reactive power and active power showed different patterns after the fault occurrence, depending on the wake effects.

The results of this research clearly indicate that by not taking into consideration the wake effect, the reactive power and the active power might show different results, which could lead to incorrect or wrong conclusions and schemes for controlling a WPP in terms of the voltage, reactive power and active power. The results of this paper should be used as a basis for designing the control algorithms for a DFIG-based offshore WPP.

Acknowledgements

This work was supported partly by the National Research Foundation of Korea (NRF) grant funded by the Korea government (MSIP) (NO.2010-0028509) and partly by the National Research Foundation of Korea (NRF) grant funded by the Korea government (MEST) (NO.2011-0017650).

References

[1] T. Ackermann, *Wind Power in Power System*, 2nd Edition, England, John Wiley & Sons, Ltd, 2012.

[2] Global Wind Energy Council, "Global wind energy outlook 2010".

[3] F. Blaabjerg and Z. Chen, *Power electronics for modern wind turbines*, 1st ed. Seattle, WA: Morgan & Claypool, 2006.

[4] Z. Chen, J. M. Guerrero, and F. Blaabjerg, "A review of the state of the art of power electronics for wind turbines," *IEEE Trans. Power Electronics*, vol. 24, no. 8, August 2009, pp. 1859-1875.

[5] M. Liserre, R. Cardenas, M. Molinas, and J. Rodriguez, "Overview of multi-MW wind turbines and wind parks," *IEEE Trans. Industrial Electronics*, vol. 58, no. 4, April 2011, pp. 1081-1095.

[6] M. Tsili and S. Papathanassiou, "A review of grid code technical requirements for wind farms," *IET Renewable Power Generation*, vol. 3, no. 3, September 2009, pp. 308-332.

[7] J. Lopez, P. Sanchis, X. Roboam, and L. Marroyo, "Dynamic Behavior of the Doubly Fed Induction generator during three-phase voltage dips," *IEEE Transactions Energy Conversion*, vol. 22, no. 3, 2007, pp. 709-717.

[8] G. Pannell, D. J. Atkinson, and B. Zahawi, "Analytical study of grid-fault response of wind turbine doubly fed induction generator," *IEEE Trans. Energy Conversion*, vol. 25, no. 4, December 2010, pp. 1081-1091.

[9] I. Erlich, H. Wrede, and C. Feltes, "Dynamic behavior of DFIG-based wind turbines during grid faults," *Power Conversion conference Nagoya,* 2007.

[10] F. K. A. Lima, A. Luna, E. H. Watanabe, and F. Blaabjerg, "Rotor voltage dynamics in the doubly fed induction generator during grid faults," *IEEE Trans. Power Electronics*, vol. 25, no. 1, January 2010, pp. 118-130.

[11] M. Mohseni, and S.M. Islam, "Transient Control of DFIG-Based Wind Power Plants in compliance with the Australian Grid code," *IEEE Trans. Power Electronics*, vol. 27, no. 6, 2012, pp. 2813-2824.

[12] O. Anaya-Lara, N. Jenkins, J. Ekanayake, P. Cartwright, and M. Hughes, *Wind Energy Generation*: *Modeling and Control*, John Wiley & Sons, Ltd, 2009.

[13] B. Shen, B. Mwinyiwiwa, Y. Zhang, and B. Ooi, "Sensorless Maximum Power Point Tracking of Wind by DFIG Using Rotor Position Phase Lock Loop," *IEEE Trans. Power Electronics*, Vol. 24, No. 4, 2009, pp. 942-951.

[14] L. Meegahapola, T. Littler, and D. Flynn, "Decoupled-DFIG fault ride-through strategy for enhanced stability performance during grid faults," *IEEE Trans. Sustainable Energy*, vol. 1, no. 3, October 2010, pp. 152-162.

[15] I. Erlich, W. Winter, and A. Dittrich, "Advanced grid

requirements for the integration of wind turbines into the German transmission system," in *Proc. IEEE Power Eng. Soc. General Meeting* 2006, June 2006.

[16] J. Morren and S. W. H. de Haan, "Short-circuit current of wind turbines with doubly fed induction generator," *IEEE Trans. Energy Conversion*, vol. 22, no. 1, March 2007, pp. 174-180.

[17] F. Koch, M. Gresch, F. Shewarega, I. Erlich, and U. Bachmann, "Consideration of wind farm wake effect in power system dynamic simulation," in *Proc. IEEE Power Tech. Conf.*, June 2005, pp. 1-7.

[18] I. Katic, J. Højstrup, and N. O. Jensen, "A simple model for cluster efficiency," in *Proc. European wind energy association conference and exhibition*, 1986.

Jinho Kim received his B.S. degree from Chonbuk National University, Korea in 2013. He is currently pursuing his M. S. degree at Chonbuk National University. He is also an assistant researcher at the WeGAT Research Center. His research interests include the development of control and protection methods for wind power plants.

Jinsik Lee received his B.S. and M.S. degrees from Chonbuk National University, Korea in 2011 and 2013. He is currently pursuing his Ph. D. degree at Chonbuk National University. He is also an assistant researcher at the WeGAT Research Center. His research interest includes plant control systems for wind power plants.

Yongsug Suh received B.S. and M.S. in Electrical Engineering from Yonsei University, Seoul, Korea, in 1991 and 1993, respectively, and his Ph.D. in Electrical Engineering from the University of Wisconsin, Madison, WI, USA, in 2004. Since 2008, he has been with the Department of Electrical Engineering, Chonbuk National University, Jeonju, Korea, where he is currently an Associate Professor. His current research interests include the power conversion systems of high power for renewable energy sources and medium voltage electric drive systems.

Byongjun Lee received B.S. degree from Korea and Ph.D degrees in Electrical Engineering from Iowa State University in 1991 and 1994 respectively. He is currently a professor in the Dept. of Electrical Engineering at Korea University. His interests include power system operation, voltage control, system protection schemes (SPS), PMU and large-scale wind farm integration

Yong Cheol Kang received his B.S., M.S., and Ph.D. degrees from Seoul National University, Korea, in 1991, 1993, and 1997, respectively. He has been with Chonbuk National University, Korea, since 1999. He is currently a professor at Chonbuk National University, Korea, and the director of the WeGAT Research Center. His research interests include the development of new protection and control systems for wind power plants.